Point-Source Localization in Blurred Images by a Frequency-Domain Eigenvector-Based Method

Metin Gunsay and Brian D. Jeffs, *Member, IEEE*

Abstract—In this paper, we address the problem of resolving and localizing blurred point sources in intensity images. Telescopic star-field images blurred by atmospheric turbulence or optical aberrations are typical examples of this class of images. A new approach to image restoration is introduced, which is a generalization of 2-D sensor array processing techniques originating from the field of direction of arrival estimation (DOA). It is shown that in the frequency domain, blurred point source images can be modeled with a structure analogous to the response of linear sensor arrays to coherent signal sources. Thus, the problem may be cast into the form of DOA estimation, and eigenvector based subspace decomposition algorithms, such as MUSIC, may be adapted to search for these point sources. For deterministic point images the signal subspace is degenerate, with rank one, so rank enhancement techniques are required before MUSIC or related algorithms may be used. The presence of blur prohibits use of existing rank enhancement methods. A generalized array smoothing method is introduced for rank enhancement in the presence of blur, and to regularize the ill posed nature of the image restoration. The new algorithm achieves inter pixel super-resolution and is computationally efficient. Examples of star image deblurring using the algorithm are presented.

I. INTRODUCTION

POINT source image restoration as defined in this work is the problem of resolving individual points, or impulses, in an image that has been corrupted by noise and by convolution with some blurring function. The point spread function (PSF) of the imaging system can merge closely located points to the extent that they can not be resolved in the presence of noise without some form of super-resolution provided by the restoration algorithm.

The point source image problem is a special case of image restoration where it is known or assumed *a priori* that the true image is sparse or point-like. Judicious use of this prior image model in developing the restoration algorithm will yield greatly superior results over what can be obtained from more conventional general purpose methods [1]. The eigenvector based approach presented here depends on this underlying point-like structure of the true image, and is closely related to methods used for source localization in sensor array processing.

Point source images are encountered in the fields of astronomical image restoration, biomedical imaging, and echo

resolution, to mention a few examples. Deblurring of star fields is one of the major applications, and will be the emphasis of the discussion to follow. Blur in long exposure astronomical star images may be due to atmospheric turbulence, misfocus, poor telescope tracking, finite aperture size, or other optical distortion effects. Atmospheric turbulence can cause nearby stars to become blurred beyond resolution so as to appear as a single star.

A. Problem Formulation

Since we wish to localize point sources in images to arbitrarily fine resolution, we begin with a common continuous space model for an observed image, corrupted by noise and a 2-D convolutional blur

$$g(x,y) = h(x,y) * f(x,y) + \eta(x,y) \tag{1}$$

where $\eta(x,y)$ is the additive observation noise and $h(x,y)$ is the blurring PSF. Because the desired true image, $f(x,y)$, is point-like, and sparse, the convolutional blur yields a finite number of shifted and scaled copies of the PSF, thus, (1) has the equivalent representation

$$g(x,y) = \sum_{p=1}^{P} u_p h(x - x_p, y - y_p) + \eta(x,y) \tag{2}$$

where u_p is the amplitude of the pth image point and P is the total number of point sources seen in the image.

We will assume that we have access to $g(x,y)$ only through a discrete-space sampling process, i.e., we observe the sampled image $g[i,k] = g(i\Delta_x, k\Delta_y)$, where Δ_x and Δ_y are the spatial sample intervals. It will be convenient to adopt a row scanned vector notation for an $M_1 \times M_2$ pixel window of $g[i,k]$

$$
\begin{aligned}
\mathbf{g} &= [g_1, \ldots, g_M]^T \\
&= [g[0,0], \ldots g[0, M_2 - 1], g[1,0], \ldots g[1, M_2 - 1], \\
&\quad \ldots g[M_1 - 1, M_2 - 1]]^T.
\end{aligned} \tag{3}
$$

g has length $M_1 \times M_2 = M$. In order to accommodate image sequence data (e.g. video or multiframe exposures) as well as a single frame images, a time index may be added to image vectors, e.g. $\mathbf{g}(t)$. It will be assumed in the following development that $f(x,y)$ does not change with time, but that only noise fluctuations contribute to the time dependence of $\mathbf{g}(t)$. This model is consistent, for example, with a series of long exposure telescopic star images, where true star intensities do not fluctuate, atmospheric turbulence is averaged over the exposure time to give a repeatable blur PSF, and noise is

independent from frame to frame. In the remainder of this paper we will ignore the time index for convenience, and indicate later how to incorporate multiple frames into the algorithm.

The problem addressed by this paper is to recover $f(x, y)$ from the observation g, or equivalently to estimate image parameters (x_p, y_p) and u_p. Though the observed image is discrete, position parameters x_p and y_p are continuous and separation between points may be less than the pixel spacing. This will require an algorithm capable of super resolution.

B. Related Work

Eigenvector techniques applied to image processing are quite new. Aghajan *et al.* use an eigenvector based approach to model the problem of finding the orientation of crisscrossed lines in an image, and they solve it with a variation of the traditional MUSIC algorithm which originates from the DOA problem [2]. Also, Mosher *et al.* perform 3-D localization of independently fluctuating current dipoles within the brain from magnetoencephalogram (MEG) data using eigenvector based techniques [3]. Tewfik and Deriche have used a frequency domain eigenstructure approach for edge detection, but perform their processing in 1-D row or column strips rather than the true 2-D approach presented here [4]. Bruckstein addresses the 1-D case of this problem using eigenvector based techniques in the time domain but makes the assumption that point magnitudes are randomly fluctuating and thus, a covariance matrix formed from the observed sequence has a rank equal to the number of sources in the sequence [5].

In our problem of interest, this common assumption of source independence will not hold. For example, in the case of astronomical imaging, the unblurred intensity of stars does not fluctuate over a sequence of several snapshots; rather, the observed time variations are due to noise or time variations of the blur. More importantly, if we are to succeed in restoring single frame images, we cannot rely on random source fluctuations over time to build up covariance matrix rank.

We have assumed in our formulation that though $g(t)$ is time dependent, $f(x, y)$ is not. This deterministic model for $f(x, y)$ is analogous to the fully coherent scene case found in the DOA literature, and requires special techniques to build up the degenerate rank of the associated autocovariance matrix before eigendecomposition methods may be applied. Shan *et al.* introduced a widely used method based on smoothing (averaging) over subarrays for rank enhancement in the case of coherent scene processing of uniform line array data [6]. Yeh *et al.* showed how array smoothing could be use for 2-D arrival angle estimation with uniform 2-D sensor arrays [15]. We introduce a new 2-D rank enhancement method which extends array smoothing to the case of nonuniform weighting of sensor responses, which, for image restoration problems, is due to the blur PSF. By transforming the image into the frequency domain, we exploit the fact that shifts in the spatial domain of a blurring function result in phase shifts across all of the elements of the image in the frequency domain. This yields a signal structure similar to 2-D array DOA problems, but

where there is a nonuniform weighting across sensor (pixel) elements due to blur.

Other techniques have been designed explicitly for point source image restoration. One of the earliest applied to astronomical star images is CLEAN [7]. While this algorithm is computationally efficient and well suited to point images, it can produce extraneous stars and other artifacts. The l_p-simplex search algorithm [1] is a nonlinear optimization theoretic technique which maximizes a sparseness objective function over a constraint set. Because sparseness objective functions are typically concave, the solutions given by the algorithm may be local minima only.

The remainder of this paper is organized as follows: For background information, a tutorial discussion on subspace methods as applied to DOA estimation with sensor arrays is presented in Section II. The new algorithm is developed in Section III. Section IV gives examples of the algorithm as applied to synthetic star fields and actual astronomical image data. Section V presents conclusions and observations.

II. SUBSPACE METHODS AND SPATIAL SMOOTHING IN SENSOR ARRAY PROCESSING

Since the new image restoration algorithm relies heavily on a theoretical foundation borrowed from sensor array processing, this brief tutorial introduction is presented to motivate the discussion and introduce notation. DOA estimation in the context of sensor array processing often involves determining the angular position with respect to the array of narrowband point source emitters in the far field. Subspace methods exploit the special structure of the array data covariance matrix by computing an eigenvector decomposition into orthogonal subspaces.

Given an array of N elements with wavefronts from P narrowband sources impinging upon it, the output from the array at time t may be described as

$$\mathbf{x}(t) = \mathbf{A}\mathbf{u}(t) + \eta(t) \qquad (4)$$

where $\mathbf{x}(t)$ is the observed array data vector, $\mathbf{u}(t)$ is the vector of complex random amplitudes for the P sources, the columns of $\mathbf{A}$ are the complex array response vectors corresponding to each of the P sources, $\mathbf{A} = [\mathbf{a}(\theta_1)|\mathbf{a}(\theta_2)| \cdots |\mathbf{a}(\theta_P)]$, θ_p is the direction of arrival of the pth source, and $\eta(t)$ is the additive observation noise. For the case of a uniform line array, $\mathbf{A}$ is Vandermonde, with columns $\mathbf{a}(\theta_p) = [1, e^{-j\varphi(\theta_p)}, e^{-j2\varphi(\theta_p)}, \ldots, e^{-j(N-1)\varphi(\theta_p)}]^T$ where $\varphi(\theta)$ is a function mapping source direction to inter-element electrical phase at the array. This particular structure for $\mathbf{A}$ is required for the spatial smoothing method described below. The autocovariance of $\mathbf{x}(t)$ (assuming zero mean data) is given by

$$\mathbf{R} = E\{\mathbf{x}(t)\mathbf{x}^H(t)\} = \mathbf{A}\mathbf{R}_u\mathbf{A}^H + \Sigma \qquad (5)$$

where ^{H} represents the complex conjugate transpose, $\mathbf{R}_u$ is the autocovariance of u, and Σ is the noise autocovariance. If the noise is uncorrelated element to element and of equal variance, σ_η^2, then $\Sigma = \sigma_\eta^2 \mathbf{I}$. If the P sources are mutually incoherent, the matrix $\mathbf{A}\mathbf{R}_u\mathbf{A}^H$ will be of rank P.

Eigenvector algorithms decompose $\mathbf{R}$ into two orthogonal subspaces: $\mathbf{E}_s$ and $\mathbf{E}_n$, the signal and noise subspaces, respectively, by solving the partitioned generalized eigenvector problem

$$\mathbf{R}[\mathbf{E}_s \mid \mathbf{E}_n] = \Sigma[\mathbf{E}_s \mid \mathbf{E}_n]\Lambda \qquad (6)$$

where Λ is the diagonal eigenvalue matrix. $\mathbf{E}_s$ contains the eigenvectors corresponding to $\mathbf{A}\mathbf{R}_u\mathbf{A}^H$, and $\mathbf{E}_n$ contains the remaining eigenvectors. Partitioning the eigenvectors into $\mathbf{E}_s$ and $\mathbf{E}_n$ is particularly easy if $\Sigma = \mathbf{I}\sigma_n^2$ and σ_η^2 is less than the power in the smallest signal component. In this case, eigenvalues are ordered in descending magnitude, and the eigenvectors corresponding to the P largest elements of Λ are then selected for $\mathbf{E}_s$. If P is unknown, it may be estimated by any of several different methods (e.g., the minimum description length [12]).

The signal subspace spans the same space as $\mathbf{A}$, and since $\mathbf{E}_n$ is orthogonal to $\mathbf{E}_s$, the noise space is orthogonal to the array responses of the P sources. The algorithm searches for the $\mathbf{a}(\theta)$ which are most orthogonal to the noise space, and these vectors correspond to the directions of arrival of the sources.

A number of eigenstructure based methods exist that exploit this orthogonality property in order to estimate θ_p. We will focus our attention on the well known MUSIC algorithm [11] for illustrative purposes, but others, like the minimum norm method [8] would be suitable for the image restoration formulation developed in the following section. The MUSIC spectrum is defined as

$$P_{\mathrm{MU}}(\theta) = \frac{\mathbf{a}(\theta)^H \mathbf{a}(\theta)}{\mathbf{a}(\theta)^H \mathbf{E}_n \mathbf{E}_n^H \mathbf{a}(\theta)} \qquad (7)$$

where $\mathbf{a}(\theta)$ is a proposed steering vector at angle θ. The θ values which correspond to the peaks of the spectrum, $P_{\mathrm{MU}}(\theta)$, are the estimated direction of arrival angles.

Eigenvector based methods fail if the sources are coherent because $\mathbf{R}_u$ does not have full column rank. However, this may be overcome in uniformly spaced line arrays using spatial smoothing [6]. This method increases the rank of the signal sub-space of $\mathbf{R}$ by averaging together the autocovariance matrices of shorter subarrays, and takes advantage of the fact that the data in each subarray is just a phase shifted copy of the other subarrays. L distinct (though overlapping) subarrays may be defined for an N element line array as follows, $\mathbf{x}_i(t) = [x_i(t), x_{i+1}(t), \ldots, x_{N-L+i}(t)]^T$, $1 \le i \le L$. Due to the Vandermonde structure of $\mathbf{A}$ for uniform line arrays, the relationship between subarrays may be expressed as $\mathbf{x}_i(t) = \mathbf{A}\mathbf{C}^{i-1}\mathbf{u}(t) + \mathbf{n}_i(t)$, where $\mathbf{C}$ is a diagonal matrix given by $\mathbf{C} = \mathrm{diag}\{[e^{-j\varphi(\theta_1)}, e^{-j\varphi(\theta_2)}, \ldots, e^{-j\varphi(\theta_P)}]\}$. Spatial smoothing consists of averaging across the autocovariance matrices of each subarray, which yields

$$\bar{\mathbf{R}} = \frac{1}{L}\sum_{i=1}^{L} E\{\mathbf{x}_i(t)\mathbf{x}_i^H(t)\}$$

$$= \mathbf{A}\left[\frac{1}{L}\sum_{i=1}^{L}\mathbf{C}^{i-1}\mathbf{R}_u(\mathbf{C}^{i-1})^H\right]\mathbf{A}^H + \frac{1}{L}\sum_{i=1}^{L}\Sigma_i. \quad (8)$$

$$= \mathbf{A}[\bar{\mathbf{R}}_u]\mathbf{A}^H + \bar{\Sigma}$$

It can be shown that if $L > P, \bar{\mathbf{R}}_u$ has rank equal to P and retains the desired phase information for each source [6]. Thus eigenvector based methods may be applied directly to the smoothed autocovariance matrix $\bar{\mathbf{R}}$.

III. ALGORITHM THEORETICAL DEVELOPMENT

In this section we transform the imaging model expressed by (2) into a form which can be solved with traditional DOA estimation techniques.

A. Frequency-Domain Signal Model

In order to map spatial shifts of source position into the phase shifts needed by the eigenstructure decomposition algorithm, g is first transformed into the frequency domain. The 2-D spatial DFT of g may be computed in row-scanned vector form by multiplying g by $\mathcal{F}$, a truncated version of the 2-D DFT matrix,

$$\tilde{\mathbf{g}} = \mathcal{F}\mathbf{g}. \qquad (9)$$

The observed image is real, so its 2-D DFT has conjugate symmetry, half of the elements contain redundant information, and the order of the system can be reduced by half without loss of resolution. To do so, $\mathcal{F}$ is formed from the last $N = M/2$ rows (assuming M_1 and M_2 are even, the odd case is handled similarly) of a frequency unwrapped version of the standard 2-D DFT transform matrix [14]

$$\mathcal{F} = \mathbf{F}^{\mathrm{row}} \otimes \mathbf{F}^{\mathrm{col}}$$

where $\otimes$ is the Kronecker product, and matrices $\mathbf{F}^{\mathrm{row}}$ and $\mathbf{F}^{\mathrm{col}}$ have elements[1]

$$F_{i,k}^{\mathrm{row}} = e^{-j2\pi ik/M_1}, 0 \le i \le M_{1U}, M_{1L} \le k \le M_{1U},$$

where

$$M_{1L} = \frac{-M_1}{2}, M_{1U} = \frac{M_1}{2} - 1,$$

$$F_{i,k}^{\mathrm{col}} = e^{-j2\pi ik/M_2}, M_{2L} \le i, k \le M_{2U},$$

where

$$M_{2L} = \frac{-M_2}{2}, M_{1U} = \frac{M_2}{2} - 1.$$

Thus, $\mathcal{F}$ has size $N \times M$. Multiplying a row scanned image vector by $\mathcal{F}$ yields a frequency domain representation of the image which is "unwrapped" (dc term in the center), a condition necessary for fractional pixel resolution [19].

In order to identify the point position information contained in $\tilde{\mathbf{g}}$, we will compare (9) to a sampled version of the continuous-space Fourier transform of (2). The Fourier transform of $g(x,y)$ is

$$G(\omega_1, \omega_2) = \sum_{p=1}^{P} u_p e^{-j(\omega_1 x_p + \omega_2 y_p)} H(\omega_1, \omega_2) + \eta(\omega_1, \omega_2). \qquad (10)$$

[1] Note that we have allowed the matrix indexes to range over both negative and and positive integers to simplify notation, e.g., $i = M_{2L}$ is the first row of $\mathbf{F}^{\mathrm{col}}$.

Since g is created by a windowed sampling of $g(x,y)$, if we assume $g(x,y)$ is zero outside the window of interest, then the qth element, $\tilde{g}_q$, of $\tilde{g}$ is related to $G(\omega_1, \omega_2)$ as follows

$$\tilde{g}_q = \frac{1}{\Delta_x \Delta_y} \sum_{l=-\infty}^{\infty} \sum_{r=-\infty}^{\infty} G\left(\frac{i2\pi}{\Delta_x M_1} + \frac{l2\pi}{\Delta_x}, \frac{k2\pi}{\Delta_x M_2} + \frac{r2\pi}{\Delta_y}\right)$$

where $q = iM_2 + k - M_{2L} + 1$ for $0 \leq i \leq M_{1U}, M_{2L} \leq k \leq M_{2U}$. Substituting (10) into this result yields the approximate relationship

$$\tilde{g}_q \approx \frac{1}{\Delta_x \Delta_y} \sum_{p=1}^{P} u_p e^{-j2\pi\left(\frac{1}{M_1\Delta_x} x_p \frac{k}{M_2\Delta_y} y_p\right)}$$
$$\times H\left(\frac{2\pi i}{M_1\Delta_x}, \frac{2\pi k}{M_2\Delta_y}\right) + \eta\left(\frac{2\pi i}{M_1\Delta_x}, \frac{2\pi k}{M_2\Delta_y}\right). \quad (11)$$

The approximating assumption has been made that $H(\omega_1, \omega_2)$ is band limited so no aliasing occurs and the summations over l and r may be dropped. Though requiring our observation to be zero outside the sampling window conflicts with this approximation, (11) holds with negligible error for most blurs of interest, which typically have a finite region of support and are low pass. A detailed analysis of the estimation error due to aliasing $H(\omega_1, \omega_2)$ when these assumptions are violated is presented in [19]. It is shown that these effects are typically very minor.

Equation (11) has an equivalent vector-matrix representation which emphasizes the similarity between this point image model and the sensor array data model of (4)

$$\tilde{g} = \mathbf{HVu} + \tilde{\eta} \quad (12)$$

where we have the equation at the bottom of the page.

$$\mathbf{V} = [\mathbf{v}_{x_1,y_1} \mid \mathbf{v}_{x_2,y_2} \mid \cdots \mid \mathbf{v}_{x_P,y_P}],$$
$$\mathbf{v}_{x_p,y_p} = \mathbf{v}_{x_p} \otimes \mathbf{v}_{y_p}$$
$$\mathbf{v}_{x_p} = \left[1, e^{-j2\pi\left(\frac{1}{M_1\Delta_y} x_p\right)}, \ldots, e^{-j2\pi\left(\frac{M_{1U}}{M_1\Delta_y} x_p\right)}\right]^T,$$
$$\mathbf{v}_{y_p} = \left[e^{-j2\pi\left(\frac{M_{2L}}{M_2\Delta_y} y_p\right)}, \ldots, 1, \ldots, e^{-j2\pi\left(\frac{M_{2U}}{M_2\Delta_y} y_p\right)}\right]^T$$
$$\mathbf{u} = \frac{1}{\Delta_x \Delta_y}[u_1, \ldots, u_p]^T.$$

Some interpretation of (12) will be helpful here. Source position information is contained in the phase structure of $\mathbf{V}$, which plays the same role as $\mathbf{A}$ in (4). Both matrices consist of columns of incremental, exponential phase vectors, with the pth column corresponding to the pth point source. Note

that x_p and y_p are continuous variables which permit sub-pixel position information to be represented. Though $\mathbf{V}$ is not Vandermonde, it will be shown to have sufficient structural regularity to enable a form of smoothing. As in (4), $\mathbf{u}$ contains source amplitude information. The autocovariance matrix of $\tilde{g}$ is now seen to be of the form

$$\mathbf{R}_{\tilde{g}} = \mathbf{HVR}_u \mathbf{V}^H \mathbf{H}^H + \Sigma \quad (13)$$

which is clearly similar to (5).

There are, however, some significant differences between the DOA estimation and point image restoration problems. Diagonal matrix $\mathbf{H}$ is the sampled Fourier transform of the blurring PSF, and imposes a nonuniform weighting on pixels of $\tilde{g}$ not found in (4). In (12), $\mathbf{u}$ is not time-varying or random, so sources are seen as correlated, and some form of smoothing is always required to build system rank. Also, the nonuniform weighting of $\mathbf{H}$ in (12) prohibits using known array smoothing methods.

B. Generalized 2-D Smoothing

This section introduces a new technique which is a generalization of spatial smoothing involving averaging in the frequency domain over the autocovariance matrices of subimages. This is analogous to the sub-array smoothing introduced by Yeh et al for 2-D sensor arrays [15], but an additional operation is required to deal with the nonuniform weighting caused by the image blur.

Fig. 1 shows how a $\Theta_1 \times \Theta_2$ pixel sub-image is extracted from a larger image, and how elements are arranged into an ordered vector. Note that in (12) $\tilde{g}, \tilde{\eta}$, each of the columns of $\mathbf{V}$, and the diagonal of $\mathbf{H}$, are all colexigraphically ordered frequency domain image vectors. The subscript $[m, n]$ will be applied to these variables to refer to the subimages whose upper left corners are at position (m, n) in the corresponding 2-D images. For example, subimages of $\tilde{g}(t)$ are defined as

$$\tilde{\mathbf{g}}_{[m,n]} = [\tilde{g}_{m,n}, \tilde{g}_{m,n+1}, \ldots, \tilde{g}_{m,n+\Theta_2-1}, \tilde{g}_{m+1,n}, \tilde{g}_{m+1,n+1},$$
$$\ldots, \tilde{g}_{m+1,n+\Theta_2-1}, \ldots, \tilde{g}_{m+\Theta_1-1,n}, \tilde{g}_{n+\Theta_1-1,n+1},$$
$$\ldots, \tilde{g}_{m+\Theta_1-1,n+\Theta_2-1}]^T$$

and (12) has the corresponding subimage representation

$$\tilde{\mathbf{g}}_{[m,n]} = \mathbf{H}_{[m,n]} \mathbf{V}_{[m,n]} \mathbf{u} + \tilde{\eta}. \quad (14)$$

We will use L to indicate the total number of subimages used in generalized smoothing. When all possible subimages of size $\Theta_1 \times \Theta_2$ are used, $L = (M_{1U} - \Theta_1 + 2)(M_2 - \Theta_2 + 1)$, though

$$\mathbf{H} = \begin{bmatrix} H\left(0, \frac{2\pi M_{2L}}{M_2\Delta_y}\right) & & & & \\ & H\left(0, \frac{2\pi(M_{2L}+1)}{M_2\Delta_y}\right) & & & 0 \\ & & \ddots & & \\ & 0 & & & \\ & & & & H\left(0, \frac{2\pi M_{1U}}{M_1\Delta_x}, \frac{2\pi M_{2U}}{M_2\Delta_y}\right) \end{bmatrix}$$

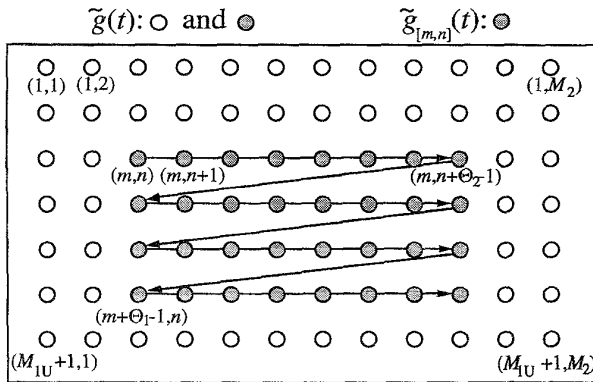$\tilde{g}(t)$: ○ and ◉ $\tilde{g}_{[m,n]}(t)$: ◉

Fig. 1. Row scanned subimage at (m, n).

as is shown in Appendix A, we may be better served by not using all possible subimages.

With this formulation we are prepared to develop a generalization of 2-D array smoothing. V is not Vandermonde as in the uniform line array case, but fortunately, there is a simple relationship between all of the $V_{[m,n]}$, which may be exploited for smoothing. We can express $V_{[m,n]}$ in terms of the product of $V_{[1,1]}$ and diagonal matrices $C_{[m,n]}$ defined as

$$C_{[m,n]} = \text{diag}\left\{ e^{-j2\pi\left(\frac{x_1(m-1)}{M_1\Delta_x} + \frac{y_1(n-1)}{M_2\Delta_y}\right)}, \right.$$
$$e^{-j2\pi\left(\frac{x_2(m-1)}{M_1\Delta_x} + \frac{y_2(n-1)}{M_2\Delta_y}\right)},$$
$$\left. \ldots, e^{-j2\pi\left(\frac{x_P(m-1)}{M_1\Delta_x} + \frac{y_P(n-1)}{M_2\Delta_y}\right)} \right\}.$$

Thus, $V_{[m,n]} = V_{[1,1]}C_{[m,n]}$ and (14) becomes

$$\tilde{g}_{[m,n]} = H_{[m,n]}V_{[1,1]}C_{[m,n]}u + \tilde{\eta}. \tag{15}$$

The corresponding autocovariance matrix is

$$R_{[m,n]} = H_{[m,n]}V_{[1,1]}C_{[m,n]}R_u C_{[m,n]}^H V_{[1,1]}^H H_{[m,n]}^H$$
$$+ \Sigma_{[m,n]}. \tag{16}$$

The $H_{[m,n]}$ blur terms in (16) are dependent on subimage indexes and prohibit achieving the simple smoothing summation form found in (8). To overcome this difficulty and to introduce a regularization operator to control noise amplification, we define a "smoothing regularization matrix", Q. Q is chosen to be an arbitrary, constant, diagonal matrix. Given a choice for Q, weighting matrices, $S_{[m,n]}$, are computed as solutions to

$$Q = S_{[m,n]}H_{[m,n]} \qquad \forall[m,n]. \tag{17}$$

Clearly one restriction on Q is that solutions to (17) must exist for all subimages $H_{[m,n]}$. Simple procedures for satisfying this constraint and for controlling the regularization effects of Q are discussed in a later section. The generalized smoothed covariance matrix is now defined as

$$\bar{R} = \frac{1}{L} \sum_{[m,n]\in B} S_{[m,n]}R_{[m,n]}S_{[m,n]}^H \tag{18}$$

where B is the set of sub-images included in smoothing. B need not include all possible sub-images. When (16) and (17)

are substituted into (18), the subimage dependent $H_{[m,n]}$ are replaced by the constant matrix Q, and the expression may be factored into a form similar to (8)

$$\bar{R} = QV_{[1,1]}\bar{R}_u V_{[1,1]}^H Q^H + \bar{S} \tag{19}$$

where

$$\bar{R}_u = \frac{1}{L} \sum_{[m,n]\in B} C_{[m,n]}R_u C_{[m,n]}^H,$$

and

$$\bar{S} = \frac{1}{L} \sum_{[m,n]\in B} S_{[m,n]}\Sigma_{[m,n]}S_{[m,n]}^H.$$

$\bar{R}$ is of size $r \times r$, where $r = \Theta_1\Theta_2$. As in the traditional DOA problem, it can be shown that with the proper choice of subimages, the rank of $\bar{R}_u$ will increase to P for each additional sub-image which is included in the average. However, unlike the 1-D case, not every distinct subimage will add to system rank, depending on the point image configuration. It is shown though in Appendix A that if B contains only subimages which are shifted diagonally with respect to each other (i.e., $m = n$ for each $[m,n] \in B$), then $\bar{R}_u$ will have rank equal to P for $L \geq P$. Thus with proper averaging and choice of Q, the first term in (19), which corresponds to the signal subspace, will be of the desired rank P. V is of full column rank, which implies that with an appropriate choice of scanning vectors, eigenvector methods can be directly applied to the smoothed autocovariance matrix $\bar{R}$.

C. Restoration Algorithm

Given this theoretical basis, we may develop a practical restoration algorithm. Though other eigenstructure techniques are applicable, we will present an algorithm based on MUSIC since it performs well and demonstrates all the important properties. The algorithm consists of the following steps:

1) Design the smoothing regularization matrix, Q.
2) Pre-compute weighting matrices, $S_{[m,n]}$.
3) Compute a sample covariance matrix, $\hat{R}$, as an estimate of $\bar{R}$.
4) Compute the generalized eigenvector decomposition of $\hat{R}$ and partition the eigenvectors into signal and noise subspaces.
5) Compute the 2-D MUSIC spectrum.
6) Perform peak detection and estimate the point amplitudes.

The design of Q will have a significant effect on algorithm performance and is dependent upon a number of factors, including the shape of the blurring function, the locations of its zeros, and the desired level of regularization. Weighting matrices, $S_{[m,n]}$, are pre-computed as solutions to (17) given knowledge of Q and $H_{[m,n]}$. Guidelines for designing Q which avoid any difficulties in solving (17) for $S_{[m,n]}$ are presented in the following section.

The smoothed sample covariance matrix is computed as an estimate of $\bar{R}$

$$\hat{R} = \frac{1}{L} \sum_{[m,n]\in B} \left(S_{[m,n]}\tilde{g}_{[m,n]} \right) \left(S_{[m,n]}\tilde{g}_{[m,n]} \right)^H \tag{20}$$

If multiple time observations of the same blurred image are available, then $\tilde{g}_{[m,n]}$ is replaced with $\tilde{g}_{[m,n]}(t)$ in (20), and an additional averaging operation is performed across the available time samples. This yields a lower variance estimate of $\mathbf{R}$. However, more commonly, only one frame is available and if this image is of sufficient size so that the number of subimages is greater than the number of sources, then (20) will provide an estimate of $\bar{\mathbf{R}}$ with the necessary rank to render a signal subspace of full rank.

Estimates of the signal and noise subspaces, $\hat{\mathbf{E}}_s$ and $\hat{\mathbf{E}}_n$, are found by using any of the readily available mathematical analysis software libraries to solve the generalized eigenvector problem,

$$\hat{\mathbf{R}}[\hat{\mathbf{E}}_s \mid \hat{\mathbf{E}}_n] = \bar{\mathbf{S}}[\hat{\mathbf{E}}_s \mid \hat{\mathbf{E}}_n]\hat{\Lambda} \qquad (21)$$

where the eigenvalues in $\hat{\Lambda}$ and their corresponding eigenvectors are ordered according to descending eigenvalue magnitudes. If the number of sources in the scene is known to be P, then $\hat{\mathbf{E}}_s$ corresponds to the P largest eigenvalues. Alternately, a number of model order estimation methods have been proposed in the literature for finding P and partitioning the signal and noise subspaces. A modified version of the minimum description length (MDL) method was used to generate results shown in Section IV [19].

The MUSIC spectrum is defined as

$$\hat{f}(x,y) = \frac{(\mathbf{Q}\mathbf{v}_{x,y})^H (\mathbf{Q}\mathbf{v}_{x,y})}{(\mathbf{Q}\mathbf{v}_{x,y})^H \hat{\mathbf{E}}_n \hat{\mathbf{E}}_n^H (\mathbf{Q}\mathbf{v}_{x,y})} \qquad (22)$$

where $\mathbf{v}_{x,y}$ is the position vector of (12), but truncated to length r. $\hat{f}(x,y)$ is a continuous function of (x,y), and may be computed at any desired sample spacing by scanning with test position vectors $\mathbf{v}_{x,y}$. If a given $\mathbf{v}_{x,y}$ corresponds to an actual point source, then it is identical to one of the columns of $\mathbf{V}_{[1,1]}$. As a result, $\mathbf{Q}\mathbf{v}_{x,y}$ lies completely in the signal subspace spanned by the columns of $\mathbf{Q}\mathbf{V}_{[1,1]}$ and $\hat{\mathbf{E}}_s$. Since $\hat{\mathbf{E}}_s$ is orthogonal to $\hat{\mathbf{E}}_n$, $\mathbf{Q}\mathbf{v}_{x,y}$, is also orthogonal to $\hat{\mathbf{E}}_n$ and causes a peak in the spectrum corresponding to an estimated point position. Once source locations are found, a simple least squares fit can be computed to estimate the amplitudes of the points.

D. Selection of the Smoothing Regularization Matrix

In (17), $\mathbf{Q}$ must be specified by the user and serves several important purposes. Without it (and the associated $\mathbf{S}_{[m,n]}$) it would not be possible to perform smoothing in the presence of a blurring function. Noise amplification and reduced aperture are two conflicting effects that must be balanced in the design of $\mathbf{Q}$. Aperture in this context refers to the region of support for pixels in $\tilde{g}$ which are effectively used in computing $\hat{f}(x,y)$. If maximum aperture is desired, then it is best to weight $\mathbf{Q}$ equally among its diagonal elements, i.e., $\mathbf{Q} = \mathbf{I}$. However, this selection of $\mathbf{Q}$ produces corresponding weighting matrices $\mathbf{S}_{[m,n]}$ that inverse filter each of the sub-images $\tilde{g}_{[m,n]}$. It is well known that the inverse filter suffers from noise amplification, due to division by very small values of the frequency domain PSF.

With these considerations in mind, there are a number ways in which $\mathbf{Q}$ may be selected. We present two simple examples of practical solutions.

1) Let

$$Q_{i,i} = \min_{[m,n]\in B} \left|(\mathbf{H}_{[m,n]})_{i,i}\right|, \qquad (23)$$

and

$$(\mathbf{S}_{[m,n]})_{i,i} = \begin{cases} \dfrac{Q_{ii}}{(\mathbf{H}_{[m,n]})_{i,i}} & |Q_{i,i}| > 0 \\ 0 & |Q_{i,i}| = 0 \end{cases} \qquad (24)$$

where the subscript ii indicates the ith element on the matrix diagonal. In practice, $(\mathbf{H}_{[m,n]})_{i,i}$ in (23) is assumed to be zero if it is small enough to cause numerical difficulties in computing the ratio in (24). Note that $0 \leq (\mathbf{S}_{[m,n]})_{i,i} \leq 1$, so this solution yields a stable regularization with no inversion problems. It also controls noise amplification and permits smoothing even if elements in $\mathbf{H}_{[m,n]}$ are zero-valued. The weighting matrices are formed with minimal computational burden because the matrices in (17) are diagonal, but some elements of $\mathbf{Q}$ may be zero, so effective aperture can be lost.

2) Another approach is to let

$$Q_{i,i} = \begin{cases} \sqrt{\dfrac{L}{\displaystyle\sum_{[m,n]\in B} \frac{1}{\left|(\mathbf{H}_{[m,n]})_{i,i}\right|^2}}} & \begin{array}{l} \text{if } |(\mathbf{H}_{[m,n]})_{i,i}| > 0 \\ \forall [m,n] \in B \end{array} \\ 0 & \text{otherwise} \end{cases} \qquad (25)$$

The corresponding $\mathbf{S}_{[m,n]}$ are computed as in (24). It is easily shown that $0 \leq (\mathbf{S}_{[m,n]})_{i,i} \leq \sqrt{L}$, again producing a stable regularization with no inversion problems.

For this second design choice for $\mathbf{Q}$, if the original noise is white ($\Sigma = \sigma_\eta^2 \mathbf{I}$), $\mathbf{Q}$ may be substituted into (17) to solve for $\mathbf{S}_{[m,n]}$ which is then used in (19) to yield

$$\bar{\mathbf{R}} = \mathbf{Q}\mathbf{V}_{[1,1]}\bar{\mathbf{R}}_u \mathbf{V}_{[1,1]}^H \mathbf{Q}^H + \sigma_\eta^2 \mathbf{I}_0 \qquad (26)$$

where $\mathbf{I}_0$ is the identity matrix with zeros in the same locations as zero valued elements of $\mathbf{Q}$. This choice of $\mathbf{Q}$ has some particularly desirable properties in addition to controlling noise amplification. Since $\bar{\mathbf{S}} = I_o$, problems of coloring the noise while smoothing are eliminated, and the eigenvector subspace partitioning problem is simplified. In addition, rather than solving for generalized eigenvectors, a simple conventional eigenvector decomposition may be used which is more efficient and computationally stable. However, Eq. (26) must first be pruned by eliminating rows and columns of $\hat{\mathbf{R}}$ corresponding to zeros on the diagonal of $\mathbf{I}_0$. $\hat{\mathbf{R}}, \mathbf{Q}$, and $\mathbf{v}_{x,y}$ in (20) and (22) are similarly pruned.

Fig. 2 illustrates graphically the effect $\mathbf{Q}$, as designed according to (25), has on array smoothing. Fig. 2(a) is the 2-D frequency domain PSF corresponding to $\mathbf{H}$. In each of Fig. 2(a)–(f), the 2-D image may be row scanned to form the diagonal elements of the corresponding matrix (i.e., $\mathbf{H}, \mathbf{H}_{[m,n]}, \mathbf{S}_{[m,n]}$, or $\mathbf{Q}$). In this example, a Gaussian blur is used for $\mathbf{H}$. Fig. 2(b) and (c) show, respectively, $\mathbf{H}_{[1,1]}$ and $\mathbf{H}_{[3,3]}$ which are two of the nine possible 10×10 pixel
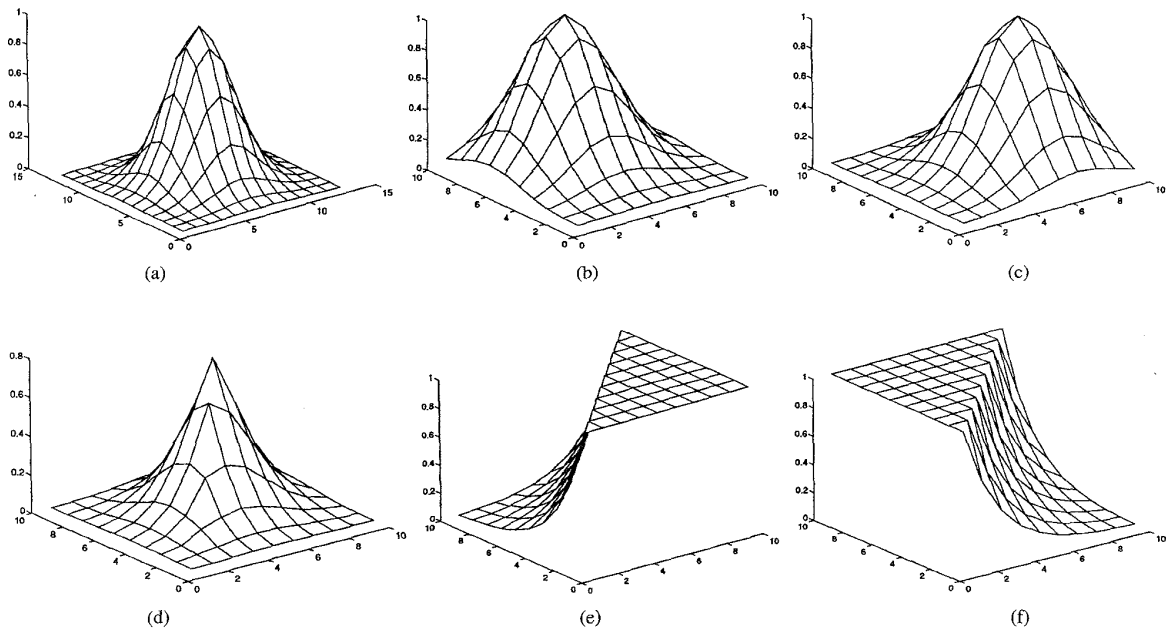
Fig. 2.   Illustrations of the effect of weighting matrices on PSF subimages. (a) 2-D representation of the diagonal elements of $\mathbf{H}$. (b) Subimage PSF $\mathbf{H}_{[1,1]}$. (c) Subimage PSF $\mathbf{H}_{[3,3]}$. (d) Smoothing regularization matrix, $\mathbf{Q}$. (e) Weighting matrix $\mathbf{S}_{[1,1]}$. (f) Weighting matrix $\mathbf{S}_{[3,3]}$. Note that $\mathbf{S}_{[1,1]}\mathbf{H}_{[1,1]} = \mathbf{Q}$ and $\mathbf{S}_{[3,3]}\mathbf{H}_{[3,3]} = \mathbf{Q}$. This yields a constant sub-image blur function allowing smoothing to take place.

subimages of $\mathbf{H}$. In order to perform array smoothing, each subimage PSF must be weighted by a corresponding $\mathbf{S}_{[m,n]}$ so that the resulting weighted PSF is constant with respect to $[m, n]$. Fig. 2(e) and (f) shows $\mathbf{S}_{[1,1]}$ and $\mathbf{S}_{[3,3]}$, respectively, which are used to scale $\mathbf{H}_{[1,1]}$ and $\mathbf{H}_{[3,3]}$ of Fig. 2(b) and (c). The resulting subimage, $\mathbf{Q} = \mathbf{S}_{[m,n]}\mathbf{H}_{[m,n]}$ is independent of the PSF, and is shown in Fig. 2(d). Note that $\mathbf{Q}$ contains small values wherever any of the $\mathbf{H}_{[m,n]}$ have a corresponding small value. This insures that no noise amplification occurs in the pixels during the restoration process, but does limit the effective aperture.

IV. RESULTS

Algorithm performance is demonstrated in this section by applying the method to several blurred single frame star cluster images. In the first example, an actual telescopic image of a star cluster is processed. Fig. 3(a) shows the original image with blur due to atmospheric turbulence and an optical aberration in the telescope which produces a "donut" shaped PSF. The PSF was estimated from a nearby isolated star in the same image [outside the field of view of Fig. 3(a)]. Fig. 3(c) presents the resulting music spectrum, which shows peaks at locations corresponding to estimated star positions, while Fig. 3(d) is a least squares amplitude fit at the detected peaks from 3(c). The algorithm determines that there are four stars present and estimates their locations. It is difficult to tell if the reconstructions of actual star images are correct, because we usually have no access to the true image, and can only compare the results against other algorithms. In this example there is an elongated diagonal feature of unknown structure. The restored image identifies this as consisting of two stars, locates these
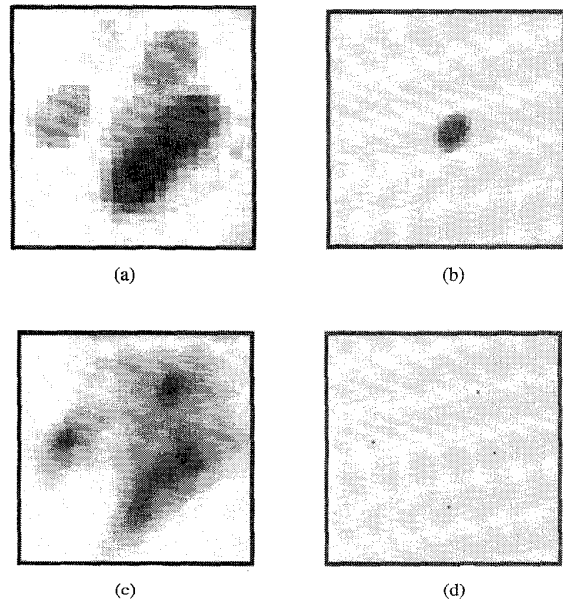

Fig. 3.   Reconstruction of an actual star cluster with an unusual blurring function. Black corresponds to highest intensity. (a) Blurred image. (b) PSF. (c) MUSIC spectrum. (d) Least-square fit of peaks. Figures (c) and (d) are at four times the resolution of Figs. (a) and (b). The image is from the CWRU/NOAO observatory with a 36/24 Burrel Schmidt telescope having 2.1 arc seconds/pixel resolution. The star group is in selected area 110 as cited in [17].

sources plausibly, and is consistent with the solutions obtained with maximally sparse restoration [1].

Figs. 4 and 5 present two examples of restoration of synthetic star images which are useful in evaluating performance
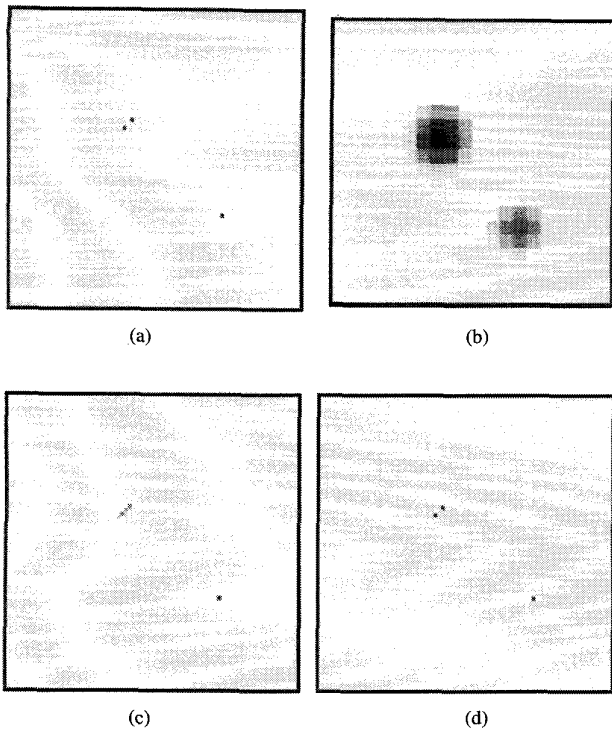
Fig. 4. Synthetic star case demonstrating super-resolution. Black corresponds to highest intensity. (a) Unblurred image. (b) Observed blurred image. (c) MUSIC spectrum. (d) Least-square fit of peaks. Fig. (a), (c), and (d) are at four time the resolution of Fig. (b).
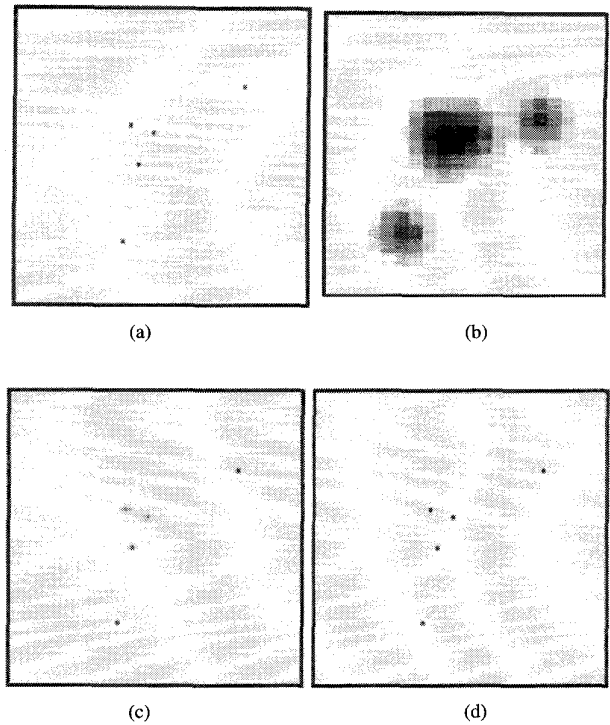

Fig. 5. Restoration of a synthetic case with five stars. Black corresponds to highest intensity. (a) Unblurred image. (b) Observed blurred image. (c) MUSIC spectrum. (d) Least-square fit of peaks. Fig. (a), (c), and (d) are at four time the resolution of Fig. (b).

because the underlying true image is known. The first synthetic case demonstrates the super-resolution capability of the algorithm. Fig. 4(a) is a cluster where two stars are separated by only half of a pixel (at the sample spacing of the observed image). The stars are blurred with a Gaussian shaped PSF with standard deviation of one observation pixel, and i.i.d. Gaussian noise is added for an SNR of 40 dB. We define the signal to noise ratio as

$$\text{SNR} = 10 \log \frac{\sigma_g^2}{\sigma_\eta^2} \qquad (27)$$

where σ_g^2 is the sample variance of g averaged over all pixels. Fig. 4(c) shows the MUSIC spectrum.

Fig. 4(d) shows the least squares fit to the peaks and demonstrates that super-resolution is possible with the algorithm. The observed image used as input to the algorithm, Fig. 4(b), was subsampled at one fourth the resolution (in each direction) of the original image of Fig. 4(a), while Fig. 4(c) was scanned at the original resolution. Though a single pixel in Fig. 4(b) is wider than the separation between stars, the algorithm recovered each star and correctly located them. The example of Fig. 5 is also a synthetic case demonstrating performance with a larger five star cluster and an SNR of 30 dB. The minimum-norm method [8] was also applied to the above examples with comparable results (not shown).

The eigenvector based restoration algorithm is compared against a regularized l_2 norm minimization solution and the CLEAN algorithm [7] in Fig. 6. The three point image of Fig. 6(b) is blurred by a Gaussian PSF with unit pixel standard

deviation, and noise is added for an SNR of 40 dB to generate the observed image in Fig. 6(a). Note that blurring is severe enough that distinct peaks are not present in the observed image. The l_2 norm minimization solution of Fig. 6(c) was found using an iterative gradient descent routine where regularization is introduced by truncating the iterations before noise amplification occurs [16]. Though this technique works quite well with many image classes, it clearly fails with this point source image example. Notice the ringing effect, and the smooth, underresolved solution, both due to the lowpass nature of the minimum l_2 objective function. This and other related techniques fail because they do not take into account the prior knowledge that the true image is point-like and sparse.

On the other hand, the simple iterative beam subtraction approach of the CLEAN algorithm was designed for restoring star images and explicitly assumes the image is point-like [7], [18]. As can be seen in Fig. 6(d), it performs better than the minimum norm approach, but it introduces an extraneous star artifact and locates the existing stars too far apart. This behavior will always occur with CLEAN when blurring is so severe that distinct peaks (or at least inflection points in the skirt of a blur function) cannot be found for each separate source point. The eigenvector-based restoration, seen in Fig. 6(e) and (f), detects and correctly locates the original three stars, and clearly outperforms the other two algorithms for this example. The maximally sparse restoration method introduced by the authors [1] also incorporates a point image prior model, but it is computationally more demanding than the eigenvector approach.
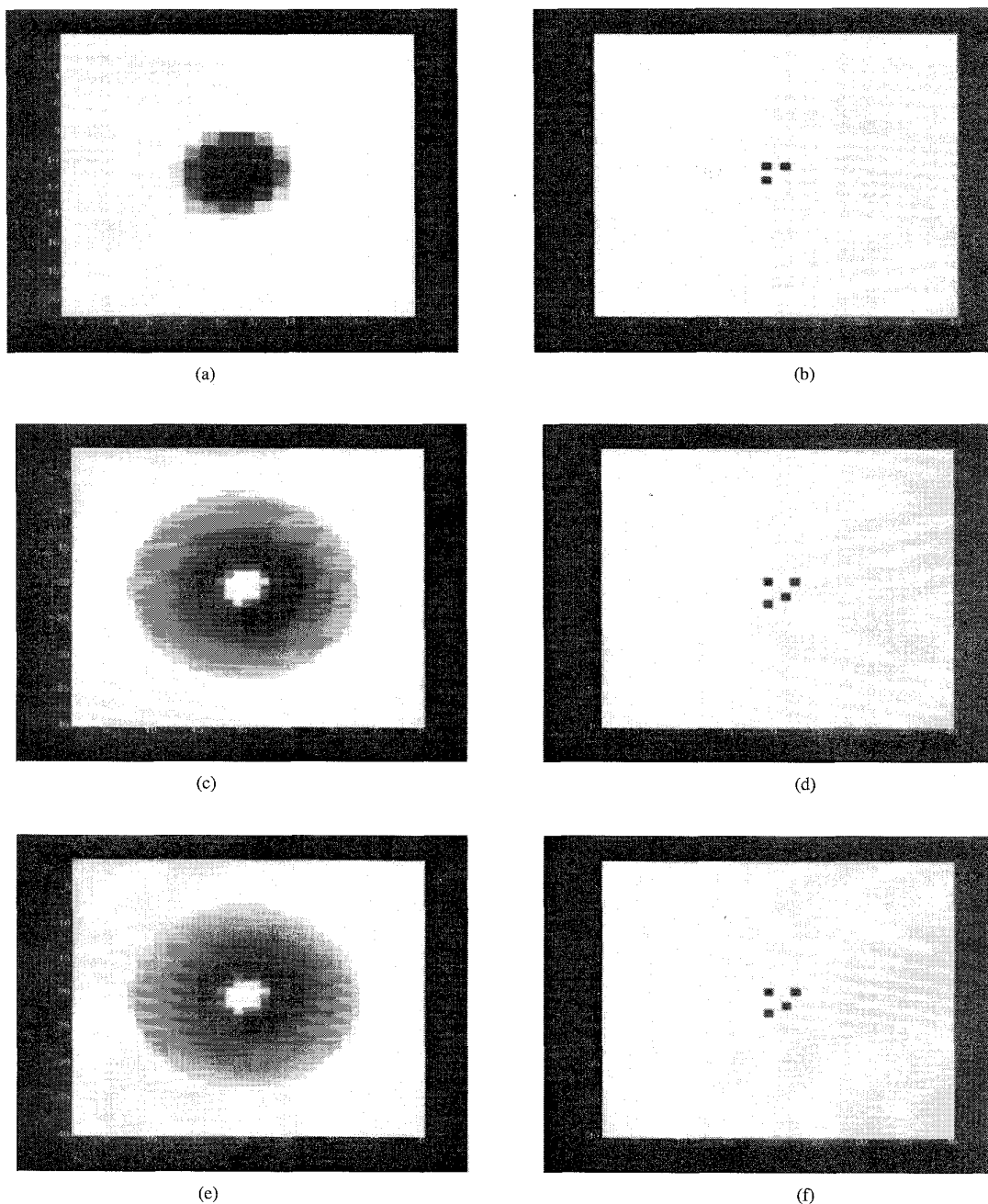
Fig. 6. Performance comparison between iterative l_2 norm minimization, CLEAN, and eigenvector based image reconstructions. Black represents highest intensity. (a) Observed blurred image with 40 dB SNR. (b) Original unblurred image. (c) Iterative minimum l_2 norm restoration with iterations truncated before onset of noise amplification. The medium gray surround near frame edges corresponds to zero, the image has some negative values. (d) CLEAN reconstruction with error threshold set at 10% of the maximum source amplitude. Lower threshold settings lead to additional extraneous stars, while higher settings eliminate stars closest to the original three. (e) MUSIC spectrum. (f) Least squares amplitude fit to all peaks in the MUSIC spectrum. This matches the original image (b).

The minimum description length method (MDL) [12] was used to solve for the number of sources in the eigenvector based image reconstructions presented above. It was necessary to modify MDL slightly from its standard form when only a single image frame (as opposed to a series of time samples) is processed. The modified MDL expression may be found in [19]. In all of the synthetic star image examples presented above, the MDL estimate of P exactly agrees with the true number of points in the image.

V. CONCLUSION

We have shown that a close relationship exists between point image restoration and the coherent scene DOA problem from array processing. Indeed, if point images are not blurred, the two problems are frequency domain duals of one another. The proposed algorithm can thus exploit the advantages of these DOA methods which have won them wide acceptance. Eigenstructure methods have been shown to approximate the

maximum likelihood (ML) solution under the prior constraint that the signal consists of point sources only, and they are computationally more efficient than the exhaustive search required by ML methods [9]. Another advantage of the algorithm is that of super-resolution, or subpixel localization and separation of points.

Since the source image data is coherent, a means of rank enhancement of the covariance matrix is needed. The proposed enhancement is a generalization of array smoothing which incorporates a regularization operator, $\mathbf{Q}$, and associated weighting matrices $\mathbf{S}_{[m,n]}$. These weighting matrices compensate for the effects of modulation introduced by the blurring function, and simultaneously provide regularization to reduce the noise amplification encountered in inherently ill posed inverse solution problems of this type. Without weighting the subimages by $\mathbf{S}_{[m,n]}$, no system rank enhancement would be possible and eigenstructure based methods would fail. Two suggested choices for $\mathbf{Q}$ were presented, each of which achieves regularization by attenuating the influence of small values in the frequency domain blur when computing the restoration. This de-emphasis of unstable terms in the system inversion is analogous to the regularization inherent in well know restoration methods, including pseudoinverse filtering, Wiener filtering, Bayesian image reconstruction, Tikhonov Miller regularized restoration, and others [14], [16].

Though this paper has focused on point image restoration, the proposed generalized smoothing method also has some obvious applications to coherent scene sensor array processing. DOA subspace methods can now be extended to problems previously considered unsuitable for array smoothing. This includes arrays with nonuniform element responses (e.g., shaded arrays) and some arrays with nonuniformly spaced sensor elements.

For example, consider the case of several correlated point sources in the far field as observed by a 2-D rectilinear sensor array with nonuniform element gains. Equation (12) can be interpreted as a model for observations from this array, with vector $\tilde{\mathbf{g}}(t)$ representing the array sample at time t, with sensor elements ordered in row-scanned form. Existing rank enhancement methods would fail here, but all that is required is to enter the (known) element gains on the diagonal of $\mathbf{H}$ in (12), specify sub-arrays, compute weighting matrices $\mathbf{S}_{[m,n]}$, and estimate the smoothed covariance matrix exactly as in (20).

APPENDIX A

In this appendix we wish to prove that if $L \geq P$ and if averaging is done only along the diagonal of the observed image, i.e., $m = n$ in $\mathbf{R}_{[m,n]}$ of Eq. (18), then generalized smoothing leads to a covariance matrix $\bar{\mathbf{R}}_u$ of rank P. This proof follows the 1-D smoothing case addressed by Pillai [13].

Since $\mathbf{u}$ is time invariant, $\mathbf{R}_u$ is a rank 1 matrix that can be represented as the diad

$$\mathbf{R}_u = \alpha \alpha^H.$$

Thus, for the case that $m = n$ for all subimages

$$\bar{\mathbf{R}}_u = \mathbf{B}\mathbf{B}^H$$

Where

$$\mathbf{B} = \begin{bmatrix} \alpha \mid \alpha \mathbf{C}_{[1,1]} \mid \cdots \mid \alpha \mathbf{C}_{[L,L]} \end{bmatrix}. \tag{28}$$

$\mathbf{B}$ may then be separated into the product of a diagonal matrix and a Vandermonde matrix.

$$\mathbf{B} = \begin{bmatrix} \alpha_1 & & & 0 \\ & \alpha_2 & & \\ & & \ddots & \\ 0 & & & \alpha_P \end{bmatrix} \begin{bmatrix} 1 & w_1^1 & w_1^2 & \cdots & w_1^{L-1} \\ 1 & w_2^1 & w_2^2 & \cdots & w_2^{L-1} \\ \vdots & \vdots & \vdots & \ddots & \vdots \\ 1 & w_P^1 & w_P^2 & \cdots & w_P^{L-1} \end{bmatrix} \tag{29}$$

where

$$w_p = e^{-j2\pi \left(\frac{x_p}{M_1} + \frac{y_p}{M_2} \right)}$$

Note that this form does not hold for $\mathbf{C}_{[m,n]}$, $m \neq n$, so the second matrix would not be Vandermonde. Clearly the rank of $\mathbf{B}$ (and thus $\mathbf{R}_u$) is the minimum of P and L since a Vandermonde matrix has rank equal to the minimum of the number of its rows or columns, and the diagonal matrix has P nonzero diagonal elements, α_p. Thus, regardless of the point configuration, $P \leq L$ points may be resolved in the image where $L = \min\{(M_{1u} - \Theta_1 + 2), (M_2 - \Theta_2 + 1)\}$ is the maximum number of diagonally shifted $\Theta_1 \times \Theta_2$ pixel subimages that can be formed from a $(M_{1U} + 1) \times M_2$ frequency domain image.

If averaging is done across other sections of the image in addition to the diagonal, then the rank may or may not increase depending upon the location of the points. For example, it is easy to show that if the stars are all located in a single row, then smoothing across a set of vertical sub-arrays will not increase the rank of $\bar{\mathbf{R}}_u$. While averaging in off-diagonal sub-images may not always increase rank signal subspace, it is often useful in creating a better estimate of $\mathbf{R}$ due to noise averaging.

ACKNOWLEDGMENT

REFERENCES

[1] B. J. Jeffs and M. Gunsay, "Restoration of blurred star field images by maximally sparse optimization," *IEEE Trans. Image Processing*, vol. 2, no. 2, pp. 202–211, Apr. 1993.

[2] H. K. Aghajan and T. Kailath, "Sensor array processing techniques for super resolution multi-line-fitting and straight edge detection," *IEEE Trans. Image Processing*, vol. 2, no. 4, pp. 454–465, Oct. 1993.

[3] J. C. Mosher, P. P. S. Lewis, and R. Leahy, "Multiple dipole modeling and localization from spatio-temporal MEG data," *IEEE Trans. Biomed. Eng.*, vol. 39, pp. 541–57, June 1992.

[4] A. H. Tewfik and M. Deriche, "An eigenstructure approach to edge detection," *IEEE Trans. Image Processing*, vol. 2, no. 3, pp. 353–68, July 1993.

[5] A. M. Bruckstein, T. Shan, and T. Kailath, "The resolution of overlapping echoes," *IEEE Trans. Acoustics, Speech and Signal Processing*, vol. 33, no. 6, pp. 1357–67, Dec. 1985.

[6] T. Shan, M. Wax, and T. Kailath, "On spatial smoothing for direction-of-arrival estimation of coherent signals," *IEEE Trans. Acoust., Speech, Signal Processing*, vol. 33, no. 4, pp. 806–11, Aug. 1985.

[7] J. A. Högbom, "Aperture synthesis with a nonregular distribution of interferometer baselines," *Astron. Astrophys. Suppl.*, vol. 15, p. 417, 1974.

[8] D. W. Tufts and R. Kumaresan, "Estimating the angles of arrival of multiple plane waves," *IEEE Trans. Aerosp. Electron. Syst.*, vol. 19, no. 1, pp. 134–39, Jan. 1983.

[9] P. Stoica and A. Nehorai, "MUSIC maximum likelihood, and Cramer-Rao bound," *IEEE Trans. Acoustics, Speech and Signal Processing*, vol. 37, no. 5, pp. 720–41, May 1989.

[10] B. D. Rao and K. V. S. Hari, "Effect of spatial smoothing on the performance of MUSIC and the minimum-norm method," in *Proc. Inst. Elec. Eng., F*, vol. 137, no. 6, pp. 449–458, Dec. 1990.

[11] R. O. Schmidt, "Multiple emitter location and signal parameter estimation," in *Proc. RADC Spectral Est. Workshop*, Oct. 1979, pp. 243–258.

[12] M. Wax and T. Kailath, "Detection of signals by information theoretic criteria," *IEEE Trans. Acoust., Speech, Signal Processing*, vol. 33, no. 2, pp. 387–92, Apr. 1985.

[13] S. U. Pillai, *Array Signal Processing*. New York: Springer-Verlag, 1989.

[14] A. K. Jain, *Fundamentals of Digital Image Processing*. Englewood Cliffs, NJ: Prentice Hall, 1989.

[15] C. Yeh, J. Lee, and Y. Chen, "Estimating two-dimensional angles of arrival in coherent source environment," *IEEE Trans. on Acoustics, Speech, and Signal Processing*, vol. 37, no. 1, pp. 153–155, Jan. 1989.

[16] R. L. Lagendijk and J. Biemond, *Iterative Identification and Restoration of Images*. Boston, MA: Kluwer, 1991.

[17] A. Landolt, "UBV photoelectric sequences in the celestial equatorial selected areas 92–115*," *Astron. J.*, vol. 789, p. 959, 1973.

[18] K. A. Marsh and J. M. Richardson, "The objective function implicit in the clean algorithm," *Astron. Astrophys.*, vol. 182, pp. 17–178, 1987.

[19] M. A. Gunsay, "Eigenvector-based point source localization applied to image restoration," Brigham Young Univ., Ph.D. dissertation, June 1994.

Metin Gunsay received B.S. and Ph.D. degrees in electrical engineering from Brigham Young University, in 1989 and 1994, respectively.

He is currently working at TransEra Corporation, Utah, developing DSP algorithms. His research interests include array processing, speech modeling, and automatic recognition of musical signals.

Brian D. Jeffs (M'90) received the B.S. and M.S. degrees in electrical engineering from Brigham Young University, in 1978 and 1982, respectively, and the Ph.D. degree in electrical engineering from the University of Southern California, in 1989.

Since 1990, he has been on the faculty of the Brigham Young University department of electrical and computer engineering, where he teaches courses in the areas of digital signal processing, digital image processing, signals and systems, and circuits. His research interests include activities in the areas of image restoration and reconstruction, biomedical imaging, array signal processing, and SONAR signal processing. From 1982–1989, he worked as a systems engineer in SONAR applications in the Anti-submarine Warfare Division of Hughes Aircraft Corporation, Ground Systems Group, Fullerton CA. From 1978–1982, he worked as a digital systems engineer at Eyring Research Institute, Provo, UT.